Catalysis Today 150 (2010) 151–162

Contents lists available at ScienceDirect

Catalysis Today

journal homepage: www.elsevier.com/locate/cattod

Problems and perspectives in nanostructured carbon-based electrodes for clean and sustainable energy☆

Gabriele Centi *, Siglinda Perathoner

Dipartimento di Chimica Industriale ed Ingegneria dei Materiali (CASPE/INSTM and ELCASS), University of Messina, Salita Sperone 31, 98166 Messina, Italy

ARTICLE INFO

Article history:
Available online 23 October 2009

Keywords:
Carbon nanotube
Electrode
PEM fuel cell
Li-ion battery
CO_2 conversion to fuel

ABSTRACT

Nanostructured carbon-based electrodes for clean and sustainable energy are of increasing relevance. This short review highlights critically some selected aspects: (i) the nanoarchitecture of the electrode, (ii) the synthesis methods and the possibility of structuring the inner nanospace of carbon nanotube, i.e. nano-in-nano design, (iii) the problem of nanointerfaces and charge transport, (iv) the interrelation between the dynamics of surface reconstruction of Pt nanoparticles under operation and charge transport limitations, (v) the multiple phenomena governing the performances of advanced electrodes for PEM fuel cells, (vi) the use of advanced nanostructured carbon-based electrodes for the electrocatalytic reduction of CO_2 to fuel, and (vii) the modification in the redox properties of transition metals via nanoconfinement within the channels of carbon nanotubes. Finally the need of introducing in catalyst design some of the recent developments made in the field of nanostructured electrodes is also commented.

1. Introduction

The issue of new solutions for clean and sustainable energy is becoming a critical factor for the future of our society [1,2]. There is a progressive depletion of fossil fuels, and at the same time an increasing concentration of greenhouse gases in the troposphere. These two factors determine the need to (i) increase the efficiency in the use of energy, (ii) develop alternative feedstocks to fossil fuels, and (iii) find innovative solutions to close the CO_2 cycle. The full transition to new sources of energy (solar energy, for example) is a process taking longer time (probably over 50 years) than that available before that climate changes could be irreversible. Therefore, it is necessary to focus R&D on those priorities, which can be critical to mitigate this transition.

The development of advanced carbon-based electrodes is a key factor for the achievement of above objectives [3–8]. Great research interest was dedicated to the development of electrodes with advanced architecture using nanostructured carbon materials (carbon nanotubes or nanofibres, ordered mesoporous materials, etc.) in contrast to the "classical" carbon materials based on graphite, glassy carbon, and carbon black. The use of carbons as electrode materials derives mainly from its structural polymorphism, chemical stability, rich surface chemistry, strong carbon–carbon bonds, and fast electron mobility.

There are several key technological areas in the energy sector, which require a better design of the electrode nanostructure using carbon based or containing materials:

(i) photo-electrochemical solar cells,
(ii) water photoelectrolysis,
(iii) photoelectrocatalytic devices for the conversion of CO_2 to fuels,
(iv) advanced Li-batteries,
(v) supercapacitors,
(vi) fuel cells.

In all these electrodes, the common problem is how to control/optimize the (1) mass and charge transport (i.e. electronic and ionic mobility), (2) electron-transfer kinetics in multi-phase boundaries, and (3) modifications on these processes, which occur upon application of a potential between the electrodes. Many of these controlling aspects are size dependent. Therefore, large attention has been dedicated to prepare nanostructured materials, based or containing carbon, due to the robustness, electrical conductivity and rich functional chemistry of the latter.

Although attention is often given to the size effect only, the problem of nanoarchitecture is equally relevant. In fact, there is a simultaneous demand of energy and power density. When high power is needed, an interfacial storage of charge such as in dielectric capacitors is necessary. As energy density becomes the key operational requirement, the choices are batteries and fuel cells. However, the simultaneous improvement of energy and power density requires a different strategy. Small devices cannot

☆ Plenary lecture at CarboCat-III, November 9–12, 2008 Berlin (Germany).

* Corresponding author.
E-mail addresses: centi@unime.it (G. Centi), perathon@unime.it (S. Perathoner).

0920-5861/$ – see front matter © 2009 Elsevier B.V. All rights reserved.
doi:10.1016/j.cattod.2009.09.009

have the surface necessary for a thin-film 2D battery or electrochemical capacitor to provide sufficient high energy. Therefore, the electrode design target is to minimize the geometric requirement, while retaining internal space of usable function, e.g. simultaneous gains in energy and power density through a proper nanoarchitecture. Rolison et al. [9] have recently emphasised the multifunctional 3D nanoarchitecture for energy storage and conversion devices. The multi-phase boundary, where all the necessary reactants (molecules, electrons, ions, and reactive surfaces) are present together for the multifunctional electrochemistry necessary to produce energy, represents often a minor fractional component of the total volume of the electrode. Therefore, the design problem is how to realize an optimal multifunctional physical space: electrons need order for high mobility, ions space (i.e., atomic-level vacancies and some disorder are necessary to increase transport rate), molecules need space to move or high solubility in a condensed phase.

Xie and Wu [10] highlighted the issue that the use of nanomaterials in electrodes brings the advantages of higher electrode/electrolyte contact area, short path lengths for ion transport, high power performance and new reactions, which are not possible with bulk materials. However, disadvantages are the increased undesirable electrode/electrolyte reactions due to high surface area, as well as the inferior packing of particles leading to lower volumetric energy densities. To solve this problem, a suitable nanoarchitecture is necessary to take synergetic advantage of the ordered building block units. In other words, an ordered array of 1D or 2D nanoobjects has different properties with respect to disordered individual nanounits themselves. Examples are the assembly of nanoparticles/nanotubes/nanowires in the desired spatial orientations to form a nanoarray, an hollow hierarchitecture or other ordered supra-nano structures [11,12].

Guo et al. [13] also emphasized the need of nano/micro hierarchical electrode materials, which can take the advantages of both nanometer-sized building blocks and of micro- or submicrometer-sized assemblies. While the former provides negligible diffusion times and hence is the key to the favourable kinetics and high capacities, the latter guarantees good stability and easy of fabrication. On the other hand, they also pointed out the several challenges remaining: (i) understand the nano-size effects, (ii) investigate the surface features of nano-objects, (iii) design optimized nano/micro structures, and (iv) search for new synthetic routes and new material systems. Liu et al. [14] recently discussed the role of oriented nanostructures (nanowire and nanotube arrays) for energy conversion and storage. They evidenced how the combination of high surface area to a controlled pore structure and alignment of the nanocrystalline phase allows optimizing electron and ion transports.

There is thus an intense research on nanostructured electrodes for applications ranging from energy storage (Li-ion batteries, supercapacitors) to energy conversion (fuel cells, solar devices). The previously cited reviews and selected others papers on these topics [15–25] provide a comprehensive coverage on these advanced materials for energy. We should remark, however, that decreasing the size to nanodimension has open new questions not fully understood, notwithstanding the large progresses made in these fields in recent years [26]. In fact, the developments have been driven mainly from phenomenological investigations, e.g. material oriented. The next necessary step is a more in depth understanding of the complex phenomena at the foundation of the physical electrochemistry and reaction/transport kinetics during operations.

For these reasons, this concise review will not discuss analytically the progresses in this field, but instead will critically highlight some selected issues or aspects in the field of clean energy related to the use of nanostructured carbon-based electrodes. We will also comment about their role in the new exciting direction of the use of electrocatalysis for the conversion of carbon dioxide to fuels [27], an area which interest is fast growing and which was indicated in a recent report of the US Department of Energy as one of the priority areas for investigation in the field of catalysis for energy [28].

2. Structuring the nanospace

Carbon nanotubes (CNT) are the natural choice to develop advanced nanostructured electrodes [8], due to various motivations: (i) the fast decrease in the cost of production, particularly for multi-wall carbon nanotubes (MWCNT), (ii) the possibility of a good tuning of the properties during the synthesis (doping with nitrogen, for example), during post-treatment (degree of graphitization, oxidative treatment, etc.) and functionalization (anchoring chemically specific organic or inorganic groups), (iii) the high aspect ratio (1D-type structure) and (iv) the high electron mobility.

Conceptually, CNT can be thought of as all sp^2 carbons arranged in graphene sheets, which have been rolled up to form a seamless hollow tube. The tubes can be capped at the ends by a fullerene type hemisphere and can have lengths ranging from tens of nanometers to several microns [29]. They can be divided into two main classes: the single wall carbon nanotubes (SWCNT) and multiwall carbon nanotubes (MWCNT). The first consists in a single hollow tube with diameters between 0.4 and 2 nm. MWCNTs are composed of multiple concentric nanotubes 0.34 nm apart, where the final MWCNT has diameters in the range of 2–100 nm. Double-wall carbon nanotubes (DWCNT) are in between SWCNT and MWCNT, but with properties closer to those of SWCNT. The conductivity of the tubes, due to their electronic properties, is important for the role of these unique nanomaterials in electrochemistry. MWCNTs are regarded as metallic conductors, a highly attractive property for an electrode. SWCNTs may be metallic, semi-conductors or small band gap semi-conductors, depending on their diameter and chirality [29,30].

The vast majority of studies used ensembles of carbon nanotubes to form nanostructured macroscopic electrodes, either with randomly dispersed nanotubes or with aligned carbon nanotubes. The first type should be processed into an electrode that maintains diffusion length, while providing electrical and mechanical contact. This could introduce penalties in terms of performances due to supplementary interfaces [14]. To preserve the benefits of electrochemistry at the nanoscale and achieve high rate capabilities, 3D nanoarchitectured electrodes are needed, which integrate electrodes and conductive substrates. The interfacial resistance and improving kinetics are thus minimized.

One of the ways for the synthesis of these nanoarchitectured materials is from hard templates, such as porous anodic aluminium oxide (AAO) and polycarbonate membranes (PCM) [31,32]. This method, which can be used for either carbon or inorganic materials, forms an ensemble of monodispersed tubular or fibrillar particles of the electrode materials, which protrude from a current collector surface like the bristles of a brush. The template method allows a precise control of both the diameter and length of the tubules or fibrils, but which is constrained from the characteristics of the template. If carbon materials would be produced, PCM or other organic membranes are not suitable. AAO are commercially available in a limited range of sizes of the channels (from 10 to 200 nm, but typically 50 to 60 nm). In addition, the aspect ratio in these channels, e.g. the ratio between length and diameter, cannot be tuned, being strongly related to the preparation method of AAO [33]. Finally, the density of the channels in AAO has strong limitations in terms of available range. The typical density of AAO is $1.3 \times 10^{10}/cm^2$ for channel size of about 50 nm. The complex (multi-step) and costly procedure, and the limitation on the

dimensions of these inorganic membranes also pose severe problems for the scale-up.

A recent interesting example is the preparation of coaxial MnO_2/carbon nanotube array electrodes for high-performance lithium batteries [34]. It is claimed that this hybrid configuration has the following advantages:

(i) improved electronic conductivity due to the presence of CNT,
(ii) homogeneous electrochemical accessibility and high ionic conductivity by avoiding agglomerative binders and other conductive additives,
(iii) well-directed 1D conductive paths due to perfect coaxial alignment,
(iv) a dual lithium storage mechanism (insertion/deinsertion in the case of CNT and formation and decomposition of Li_2O in the case of MnO_2 nanotubes).

However, the synthesis of these electrodes, schematically represented in Fig. 1, requires a complex multistep procedure. The method uses an alumina nanomembrane produced by anodic oxidation (AAO) (see the top view in the inset of Fig. 1). The AAO template is commercially available (nanopore diameter of ~200 nm and length of ~50 μm). MnO_2 nanotubes are first fabricated by vacuum infiltration inside the channels of AAO and then CNTs are grown using chemical vapour deposition. The sample is then plasma etched for 30 min to remove the amorphous carbon layer that forms during chemical vapour deposition. After a layer of an Au film (~100 nm) is sputtered onto one side of the template, which serves as the current collector for the electrode. The MnO_2/CNT hybrid coaxial structures are then released from the alumina template by dissolution in 3 M NaOH solution for 1 h, according to the authors. However, the possibility to remove completely the alumina in these conditions is questionable. The Au film prevents the coaxial hybrid structure from collapsing, after the removal of the template. The inset of Fig. 1 shows a SEM (Scanning Electron Microscopy) image of the MnO_2/CNT hybrid coaxial structure obtained by this method. These materials show about two-three times higher specific reversible charge/discharge capacity than single MnO_2 or CNT, although a fast deactivation is observed (specific capacity decreases about five times in only 15 cycles).

It should be commented that there is a very large interest in the development of improved electrodes for Li-ion batteries. These are among the most promising batteries that offer high power density and energy. However, their large-scale application is still limited by several barriers, including reliability, longevity, safety, and cost concerns. The use of nanomaterials as electrodes and electrolytes in Li-ion batteries may provide several advantages [35–37]: (i) better accommodation of the strain of lithium insertion/removal, improving the cycle life, (ii) new reactions that are not possible in bulk materials, (iii) a higher electrode–electrolyte contact area leading to a higher charge/discharge rate and thus a higher power, and (iv) a short path distance for electron and Li^+ transport, permitting the battery to operate at higher power or to use materials with low electronic/ionic conductivity without adversely affect power.

Typically, a lithium-ion battery consists of a negative electrode (NE), a positive electrode (PE), and a lithium-ion conducting electrolyte. When the cell is charged, Li ions are extracted from the PE and inserted into the NE. On discharge, the Li ions are released by the NE and taken up again by the PE. It is thus necessary to have a material that reversibly insert and deinsert with a fast kinetic and high capacity the Li ions without collapse of the structure, but at the same time that it is able for an efficient collection and transport of the electrons.

CNT are active towards electrochemical Li ion insertion. Che et al. [38] first demonstrated the reversible lithium-ion intercalation in MWCNT. However, further studies demonstrated that a progressive irreversible deactivation is present [39]. Wu et al. [40] showed that the Li insertion occurs through different mechanisms,

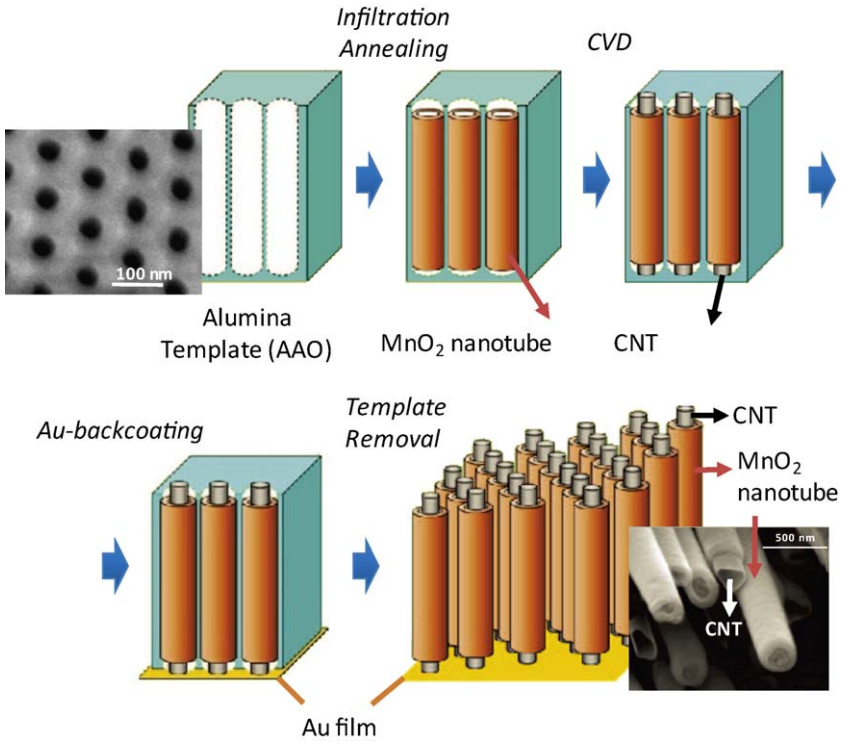

Fig. 1. Schematic diagram showing the fabrication of MnO_2/CNT hybrid coaxial nanotube arrays inside AAO template using a combination of vacuum infiltration and chemical vapor deposition techniques. A thin layer of gold (~100 nm) was sputter coated to act as current collector for the electrodes. In the insets a SEM image of a commercial alumina membrane produced by anodic oxidation (AAO) (left, top) and a SEM image of the MnO_2/CNT hybrid coaxial nanotubes (right, bottom). Adapted from Ref. [34].

i.e. in microcavities, the edges of graphitic layers and the surface of single graphitic layers, in addition to the interlayer spacing of graphitic planes. Only some of these are reversible. Eom et al. [41] evidenced that the introduction of defects in CNT facilitates the insertion of lithium ions and short-term reversibility. However, long-term reversibility (the more important from the application perspective) is an issue, because there is a progressive increase of irreversible capacity. Other problems in using CNT as electroactive materials for Li-ion batteries regard (i) the presence of a hysteresis between discharge and charge potentials, and (ii) the capacity decay during cyclic performance. The great advantage of CNT (or of similar materials such as carbon nanofibres – CNF) is that they can grow as an aligned array directly over a conductive substrate (graphite or other material) by in situ chemical vapour deposition [42,43].

Realize hybrid (nanocomposite) materials, combining the properties of CNT (or CNF) and metal-oxides (MO) nanoparticles, is the approach to improve the reversibility and capacity retention over extended cycles (>1000). At the same time, it is possible to improve the kinetics of charge/discharge. With respect to a metal-oxide array electrode prepared using the hard template method the potential advantages of using a array of CNT/MO are the following: (i) a better tunable packing density of the nanowire array to optimize the performances, (ii) a better electronic conduction due to CNF core in nanowires, and (iii) a lower complexity and cost of the preparation. Various metal oxide are suitable to give these nanocomposites and between these TiO_2 and V_2O_5 show quite interesting behaviour [44,45].

The problem is how to realize the contrasting requirements of a (i) high loading of the metal oxide in order to maximize the capacity, (ii) very low size of the metal-oxide nanoparticles (reversibility and stability improves by decreasing the size, as well as increases the surface to bulk ratio which improves the kinetics – Li diffusion in the metal oxide bulk is slower with respect to surface reaction), and (iii) good contact with the electrolyte.

Another issue regards the shape of the metal-oxide nanoparticles. Sun et al. [46] have shown that defect-rich V_2O_5 nanorolls show enhanced electrochemical properties with respect to similar, but highly ordered V_2O_5 material. The defect-rich material shows a higher number of redox sites and increased inter-layer accessibility by alkali ions, due to cracks and exfoliation. This indicates that the specific defective characteristics, in addition to the particle size, determine the electrochemical properties.

It is known that defects are stabilized decreasing the particle size, although the nanoscale form plays also a role. When the amount of defects increases above a limit, however, the electronic conduction (bulk and surface conduction) of the oxide results negatively affected [47]. In addition, a large amount of defects is negative to maintain structural integrity in several discharge–charge cycles. Therefore, it is necessary to combine high accessible nanoscale architecture to a crystalline habit, but with localized defects, which can enhance the redox and diffusion properties. At the same time, a proper nanoarchitecture would be also necessary to minimize the path of Li^+ diffusion in the electrolyte and realize an efficient contact between the metal oxide and the CNT or CNF substrate.

When the metal oxide (vanadium oxide, for example) is deposited on these carbon substrates by conventional wet procedures, an amorphous and hydrous vanadium oxide thin film forms [48] which shows a good specific Li-ion capacitance. However, the issues are (i) the still limited capacity, related to the low geometrical surface area of the 1D-type carbon substrate, and (ii) the stability during several cycles, due to the tendency to sinter of the metal-oxide film to form larger, round-shaped, particles, which have a lower surface free energy. A better interaction with the carbon support would improve the stability. Fang and Fang [49] showed that N-doped carbon nanotubes exhibit significantly enhanced properties to support vanadium oxide. There is minimal difference of capacitative performances of V_2O_5 deposited on N-doped or undoped CNT during the first cycles, but the difference becomes more marked after 1000 cycles, mainly due to sintering of the oxide. This suggests that the doping of CNT with nitrogen introduces surface functional groups, which modify the interaction (anchorage) of supported vanadium oxide with the underlying carbon substrate.

It was also shown that it is possible to use the CNT to induce the nucleation of 1D-type vanadium oxide nanostructures, with the nuclei growing into long free-standing nanorods [50]. The vanadium oxide nanorods (V_2O_x-NR) have an average length of 20 μ and diameter of 5–15 nm. The high-resolution transmission electron microscopy image of V_2O_x-NR shows an ordered crystalline structure with an average layer distance of about 0.7 nm. However, electron energy loss spectra indicate that the nanorods contain both V^{5+} and V^{4+} and X-ray diffraction patterns show the presence of a $V_2O_x{\cdot}xH_2O$ like phase instead that of V_2O_5 crystallites [50].

The CNT thus induces the nucleation of oxide nanorods stabilized by the interaction with carbon. The characteristics of supported oxide nanorods (particularly the presence of oxygen defects facilitating the insertion/deinsertion of Li as commented above) are different from those of V_2O_5 nanoparticles deposited on carbon. The CNT also provides a good electronic contact for a fast electron transport. This kind of nanoarchitecture (V_2O_x-NR grown over an host CNT) would be optimal to realize high performance Li-ion batteries, because it allows to have (i) a higher surface area and amount of metal oxide with respect to an uniform film of vanadium-oxide coating the CNT or vanadium-oxide particles supported on the CNT, (ii) a morphology (high surface to volume and high aspect ratio) favouring the Li ion charge/discharge process and contact with the electrolyte, (iii) an efficient collection and transport of electrons, and (iv) a dense packing for a high capacity. Fig. 2 schematically illustrates the procedure of synthesis of these materials, which is simpler, less costly and easier scalable of the template method shown in Fig. 1. Fig. 2 shows also the different types of supported vanadium-oxide species that could be obtained. They depend on the modalities of deposition of vanadium oxide as well as the specific characteristics of CNT. In the bottom inset of Fig. 2a TEM (transmission electron microscopy) image of a V_2O_x-NR grown over a host CNT [50] is shown, while in the top inset a SEM image of an array of CNT produced by CVD method (feeding a mixture of $FeCp_2$/toluene) is presented.

The packing density of CNT arrays produced by CVD can be tuned in a relatively large range to optimize the performances, while the template method has constrains given from the starting membrane. It is possible to control the site density of aligned carbon nanotubes from about 10^5 to $10^9/cm^2$ by controlling the method of deposition of the Ni nanoparticles acting as the catalyst for CNT growing [51]. As reference, for 100 nm diameter CNT the maximum density for a close packing is about $10^{10}/cm^2$, while about $10^{11}/cm^2$ for 30 nm CNT. Therefore, obtaining small-size carbon nanotubes or fibers allows increasing the packing density and thus the surface area. A target should be to produce MWCNT characterized by low diameter (10–20 nm) and reduced number of walls. However, it is not simple to achieve this objective.

One of the possible solutions is to use a nanoporous template for growing the CNT array. Fig. 3a shows TEM images of Fe–Co nanoparticles deposited in the channels of a mesoporous SBA-15 silica [52]. The size of these nanoparticles is about 6 nm, i.e. similar to the diameter of the SBA-15 channels. When the Fe–Co particles are located on the external surface, they have larger dimensions (about 15–20 nm). Fig. 3b shows a TEM image of a CNT prepared by CVD (feeding propane/H_2) using this catalyst. Small diameter CNT

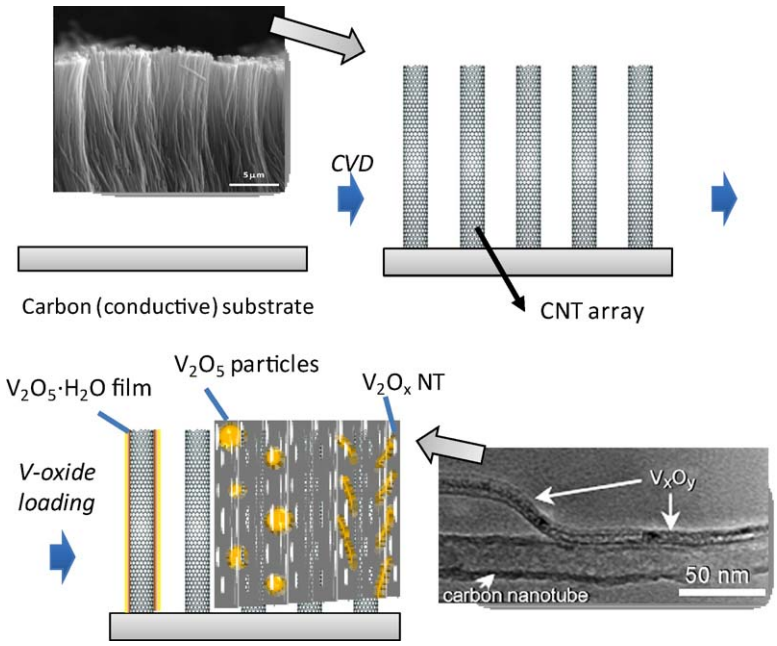

Fig. 2. Schematic diagram showing the fabrication of V_2O_x/CNT hybrid array by CVD synthesis of a CNT array and deposition of vanadium oxide by wet or other methods. Insets: (top, left) a SEM image of an array of CNT produced by CVD method (feeding a mixture of $FeCp_2$/toluene). (bottom, right) TEM image of a V_2O_x-NR growing over a host CNT. TEM image adapted from Ref. [50].

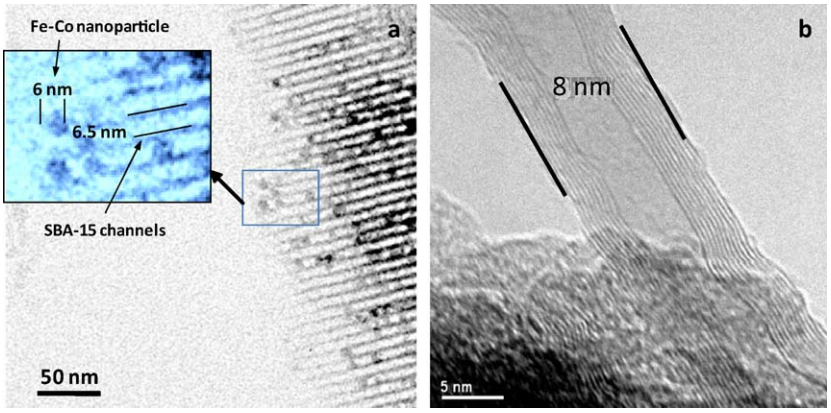

Fig. 3. (a) TEM image of the section of a SBA-15 loaded with Fe–Co (1:1) nanoparticles. In the inset, an enlarged part of the image to evidence the size of the Fe–Co nanoparticles and the diameter of SBA-15 channels. (b) TEM image of a CNT growing out of the channel of SBA-15 where a Fe–Co nanoparticle is located.

could be produced with an external diameter quite close to the diameter of the Fe–Co particles and SBA-15 channels. It is also possible to observe that the graphene sheets are well ordered parallel to the growing direction. On the contrary, the CNT, which grow on the larger Fe–Co particles located on the external surface are larger (about 40 nm) and the CNT walls are ordered at 45° with respect to the growing axes. This template method using mesoporous SBA-15 allows to control during synthesis the size of carbon nanotubes and to influence the mechanism of synthesis (from a zig-zag growing mechanism to an armchair growing mechanism). The consequence is an influence in both the electronic conduction, the reactivity towards Li ions, and the stabilization of supported metal-oxide particles.

A possibility to increase the surface area of CNT at equivalent CNT density is based on the carbon tube-in-tube (CTIT) approach [53]. In this case, there is the secondary formation of one or more tubes around a pristine nanotube. With respect to MWCNT, where the distance between the graphene layers is about 0.3 and 0.4 nm, the distance between the surfaces of the concentric carbon nanotubes is several nm, and thus it is possible for the electrolyte to enter within the space leaved from the two concentric tubes, and/or to deposit a metal oxide. By extending the method, is thus possible in theory to arrive to an array of nanotubes, each formed by a series of concentric graphene layers. This nanostructure has the potential advantage with respect to a series of stacked planar graphene layers of (i) easier fabrication, (ii) shorter distance of ion transport, and (iii) lower cost. Nevertheless, the possibility of easy mobility of ions between these concentric graphene layers has to be still demonstrated. With respect to the alternative possibility of a series of smaller tubes on the outside of backbone larger nanotubes, the advantages of CTIT concept are of (i) a higher density of packing, and (ii) better electronic transport. In fact, often when smaller CNT or CNF are grown over a carbon host macrofiber, at the interface a disordered region is present, which reduces the effectiveness of the electrical conductivity.

The CTIT could be assembled by a wet chemical reorganization of carbonaceous impurities around and inside pristine nanotubes [53]. First, the graphitic nanoparticles are disintegrated into small

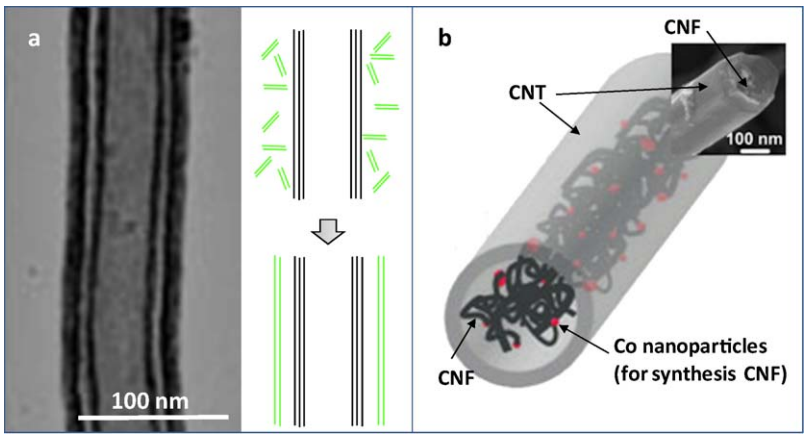

Fig. 4. (a) TEM images of CTIT with relatively small and uniform interval spaces, which exhibit similar morphologies between the inner and outer tube moieties. Such tubes are produced from the assembly of graphitic fragments around the pristine tubes, as shown in the simplified scheme. Adapted from Ref. [53]. (b) Scheme of carbon-nanotube-encapsulated carbon nanofibers (CNFs@CNTs). In the insets SEM images of the as-prepared CNFs@CNTs. Adapted from Ref. [54].

fragments by an HNO_3-based oxidation at defective sites. Secondly, the small graphene fragments are reintegrated around or inside pristine nanotubes to assemble CTIT by acid-catalyzed esterification linkages between the carboxyl and hydroxyl groups. Fig. 4a shows a transmission electron microscopy image of CTIT material that schematically illustrates the mechanism to form the second tube (by wet reorganization of the graphene fragments) on the outer surface of pristine carbon nanotubes. A similar mechanism is also possible on the inner side. The combination of the two mechanisms leads to the synthesis of triple tubular nanostructures.

An alternative procedure to prepare nano-in-nano carbon structures is based on the selective deposition of an active metal (Co nanoparticles with average size of 6.6 nm) on the inner walls of CNT (inner diameter in the 20–80 nm range), which is followed by the growth of CNF by catalytic chemical vapour deposition (using a 1:1:2 mixture of C_2H_4:H_2:He as feed) [54]. The concept is shown in Fig. 4b which also reports in the inset a SEM image of the as-prepared CNF@CNT (carbon nanofibers included in the carbon nanotube). 3D-TEM confirmed the good confinement of CNF within the CNT. The specific surface area increased from 82 to 347 $m^2\ g^{-1}$ after inclusion of CNF in the CNT, which suggests a greatly improved utilization of space inside the hollow channels of the CNT.

Using these nano-in-nano carbon materials, a new design was proposed for nanostructured electrodes in high-performance Li batteries [55]. The proposed nanoarchitectured electrode is composed of an efficient mixed-conducting network, in which CTIT serves as "electronic wire" to provide the electrons to the active materials. The tube diameter of the CTIT should be optimized to allow easy electrolyte access. Such a nanostructure provides both electronic and lithium-ion pathways, which are essential for a high rate rechargeable lithium battery. Due to the close electrical contact between the phases at the nanoscale level along the wall of the CTIT and being the material easily accessible to the electrolyte, the kinetics of Li insertion/extraction and the Li storage performance are improved over those of conventional materials [55]. We should mention, however, that still not enough proofs are available to demonstrate that mass transport inside a "crowded" CNT is really effective, and thus that may be possible to achieve the maximum possible power densities. The critical issue to solve for an effective design is to understand what is the distance between graphene layers to optimize the two contrasting aspects of shortens the distance to enhance the surface and increases the distance to facilitate the mass transport. The CTIT or CNF@CNT approaches and the alternative approach of stacked graphene sheets (see later) would have the merit at least to contribute to the understanding of this key aspect for the design of efficient Li-ion batteries.

The use of CTIT or CNF@CNT should be thus considered a possible way towards a more effective nanoenvironment with respect to CNT to increase the effectiveness of the dispersion and amount per volume of the oxide and thus the storage capacity of the battery. However, further studies are definitively necessary.

3. Nanointerfaces and charge transport

In heterogeneous catalysis, a kinetically complex multistep process involving transport and reaction steps can be simplified in terms of rate determining steps or relatively simple combination of them (effectiveness factor, in series processes). In electrocatalysis, the problem is more complex. In some cases, it is possible to identify a rate-controlling step. At low current densities, electrocatalysis may be well described by charge transfer, also in porous electrodes. The electrocatalytic reaction in these conditions obeys the Butler-Volmer (BV) equation, which describes the rate of an electrochemical reaction as a function of the departure from the equilibrium voltage of the electrochemical cell. This equation, however, fails to reproduce the behaviour of the system at high reaction rates, where nonideal effects in transport become significant [56]. Therefore, the rate is not more controlled by charge transfer in more demanding conditions as often occurs in the application of PEM (Polymer Electrolyte Membrane) fuel cells. The departures from BV behaviour, due to limitations in reactant feed, may be described using mesoscopic nonequilibrium thermodynamics [56]. The latter approach considers that the velocity coordinate has to be brought into the local-state description of the system, in order to cope with the possibility of delayed relaxations. However, fitting parameters are introduced using this approach (which is an extension of BV theory) to describe correctly the experimental results.

In fact, nano/micro-structural properties of Pt and Pt-alloy electrodes evolve during the MEA operation, as commented later. These spatiotemporal nano/microstructural changes are strongly dependent on the PEM fuel cell operating conditions. For example, surface segregation of Pt–Rh nano-clusters is dramatically altered by hydrogen chemisorption: in the absence of hydrogen, the cluster surfaces are Pt-rich, but in the presence of hydrogen, the cluster surfaces can be Rh-rich ("reversing segregation" or "reconstruction" phenomena) [57]. Therefore, limitations in H_2 diffusion to the electrode would also influence the nature of Pt-alloy clusters. On the other hand, surface charge of Pt-based

nanoparticles, due to limitations in the effectiveness of charge transport by the conductive carbon substrate, will also influence the structure of nanoparticles (directly or via induced reconstruction associated to a change in the chemisorbed species). This change would reflects also in a modification of the electrochemical double layer capacity, while in the classical BV theory the double layer structure is assumed to be uncoupled from the electrochemical reactions. BV theory cannot thus describe electron transfer reactions on nano-materials with an evolving structure and a new approach by coupling Monte Carlo simulation method for catalyst nanostructure prediction to non-equilibrium thermodynamics/mean field kinetic simulations for the calculation of the PEM fuel cell electrodes potential should be used [58], for example. Although the influence of mass transport on PEM fuel cell performances is well known [59], we should remark that often in considering the design of PEM electrodes it is assumed that electron transfer and BV theory are governing the PEM cell behaviour. The issue of mass transfer is only an engineering problem of allowing enough reactants flux to the electrodes, while there is dependence between electron-transfer kinetics in multiphase boundaries, mass transfer and electron conduction. We will discuss the relevance of these aspects in relation to the design of carbon-based electrocatalysts for PEM fuel cells.

An electrode in a PEM fuel cell is usually based on Pt metal particles supported on a conductive carbon, such as Vulcan XC-72. The Pt/C electrocatalyst is then deposited over a conductive substrate (typically carbon cloth – CC) and this composite (Pt/C/CC) is hot-pressed with a proton-conducting membrane (such as Nafion® 117) to form the so-called MEA (Membrane Electrode Assembly). The cell performance of the electrode is commonly expressed by the polarization curve, which reports the cell voltage against current density. On increasing the latter, the cell voltage decreases due to ohmic and mass transport losses [59]. The cell often operates at the maximum power density (MPD), which is the product of cell voltage and current density. Operations at lower power density are possible to have higher efficiencies. However, this would imply to increase the number of stacks at equal fuel cell power output, e.g. increase the cost. Operations with power density lower than MPD are not suitable from the application perspective, even if these conditions are often used in fundamental studies. At MPD, metal particles may become charged, when the charge transport (protons and electrons) is not efficient, and/or when the metal nanoparticle is in poor electronic contact with the carbon substrate. This effect induces a dynamic particle reconstruction to minimize the surface free energy. The effect is illustrated in the simplified model reported in Fig. 5. This model is only a simplified cartoon of a more complex phenomenon, because excess surface charge would only influence the amount of chemisorbed species, for example, which in turn influence the free surface energy and thus the optimum particle shape.

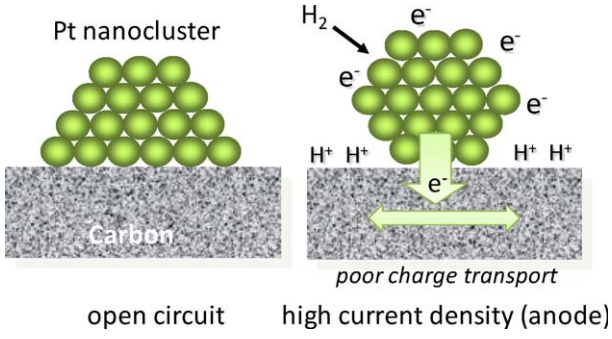

Fig. 5. Simplified model to evidence the issue of reconstruction of Pt nanoparticles in PEM fuel cells during high current density operations.

Nevertheless, Fig. 5 conceptually shows in a simplified view that the extent of dynamic reconstruction and in turn the reactivity of the metal nanoparticle strongly depends on this problem, which is related to the nature of the nanointerface and the charge transport phenomena.

Which evidences on this issue exists? Specific studies are absent, but there are some recent in situ investigations showing the presence of a reconstruction of Pt nanoparticles during PEM operations. Witkowska et al. [60] investigated by X-ray absorption fine structure (XAFS) an electrode of Pt supported on Vulcan XC-72. XAFS spectroscopy was performed in situ during PEM fuel cell operations. Changes in the near-edge structures reflecting variations in the Pt electronic structure were observed for various applied potential values in the activation region. Tada et al. [61] monitored by time-gated rapid XAFS the dynamics of surface changes in Pt nanoparticles during operations in a fuel cell. Kageyama et al. [62] evidenced by in situ XAFS that the local structure around Pt and Ru atoms in the electrocatalysts changes depending on the operation voltage.

These results evidence a restructuring of Pt particles on changing the potential, although do not proof that this change is related to an extra-charge. On the other hand, this aspect was not considered. For example, the influence on the dynamics of surface change from the interface between the metal nanoparticles and the carbon substrate in a homologous series of electrocatalysts having different polarization curves may be studied, for example.

These observations point out that in electrocatalysis, complex effects are present and there is the need of further in situ studies, which clarify the mechanism of reaction and the nature of effective working electrocatalyst more in depth. At the same time, these observations indicate that care should be taken in extrapolating results obtained in conditions of low power density or open circuit cell to high power density close circuit PEM fuel cell.

Let us clarify this issue, first recalling that Polymer Electrolyte Membrane (PEM) fuel cells are composed from an anode, where hydrogen reacts over the active electrocatalyst (Pt nanoparticles supported on carbon) to generate protons and electrons. Protons diffuse through a membrane (such as Nafion) to the cathode, which is electrically connected to the anode through a wire, which transport the electrons. At the cathode, oxygen is reduced over the active electrocatalyst (usually also Pt nanoparticles supported on carbon) to form water with the electron and protons coming from the anode.

The kinetics of cathode oxygen reduction on Pt is slow compared to the reaction of hydrogen oxidation at the anode and usually it is reported that the critical issue in PEM is to decrease the overpotential of the oxygen reduction reaction (ORR) [15,63]. This explains why a large part of research on PEM electrodes is focused on this problem. The need of a better design/development of the anode is often considered a secondary problem, or limited to the issue of improving the resistance to CO poisoning of the noble metal. It was reported, for example, "ORR contributes to a major portion (80%) of the total cell voltage losses" [15]. Based on this statement it is assumed that an improvement of both anode and cathode design is not necessary, because 'the kinetics of oxygen reduction is slower than the kinetics of hydrogen oxidation". This statement is equivalent to apply the concept of a kinetically controlling stage in a system where it should be not applied, as discussed before.

A related aspect is that the support plays a more relevant role than that of providing a good dispersion of the supported noble metal particles. Several studies on new electrodes for PEM fuel cells have been focused on the improvement of the utilization of Pt by proper support engineering, particularly on the use of advanced nanostructured carbon materials (CNT, CNF and others including nanohorns, ordered arrays of CNT or CNF, ordered mesoporous

carbon) [4,6,14,31,64]. Large differences in the behaviour and sometimes contradictory results have been observed. However, the interpretation is often related only to an influence of the support on the dispersion of the noble metal.

In order to clarify this aspect, it is useful to discuss a specific example regarding the behaviour of two anode electrodes for PEM fuel cell. Both are based on Pt/MWCNT, but in one case the carbon substrate was subjected to ball milling prior the deposition of Pt [65,66]. Ball-milling is a procedure often used to shorten and open multi-walled carbon nanotubes produced by chemical vapour deposition (CVD) method [67]. The process, however, introduces also defects, which may be evidenced by TEM images [66]. The ball milling may be considered a method to create mechanically-induced topological defects in CNT. We will indicate hereinafter as Pt/CNT_{nd} and Pt/CNT_{d} the two non-defective and defective samples, respectively.

The presence of defects improves the dispersion of Pt particles [66]. The average size of Pt particles in Pt/CNT_{d} is 1.4 nm, while Pt/CNT_{nd} shows a bimodial distribution, centred at 1 nm and 4.5 nm, respectively. The average size of Pt particles in Pt/CNT_{nd} is 3.0 nm. For reference, the mean size of Pt particles in Pt/Vulcan XC-72 electrocatalysts was found to be about 3.6 nm [68]. Therefore, in both Pt/CNT_{d} and Pt/CNT_{nd} small Pt nanoparticles (<2 nm), with the size below the usual observed in Pt/carbon black materials, are the dominant species. A more uniform distribution is observed in the Pt/CNT_{d} sample. The distribution of Pt particles allows estimating the geometrical surface area (GSA) of Pt particles, based on the assumption of a round-shaped geometry. The results are summarized in Table 1, using both the mean diameter of the particles and the size distribution. It could be observed that for Pt/CNT_{d} the difference is minimal. In Pt/CNT_{nd} showing a broader and bimodial distribution of the particle size, the difference is relevant. Note that usually, GSA is estimated only on the mean diameter of Pt particles.

The geometrical surface area determined from the particle size is an indication of the total available surface area, which depends on the dispersion of Pt on the support, but do not provide an estimation of the electrochemical active surface area. In fact, part of the Pt particles may be inactive, due to a poor contact with the carbon conductive substrate, or because part of the surface area is not accessible to the gas reactants. The estimation of the electrochemical active surface area (EAS) can be made by cyclic voltammetry (CV) experiments in acid solution, calculating the amount of charge transfer during the electroadsorption and desorption of H_2 on Pt sites [69]. The values should be corrected by the contribution of double layer charge and eventually of the support.

The values of EAS estimated in this way are also reported in Table 1. It may be noted that EAS is about 20–25% lower than the geometrical surface area (GSA), but this is reasonable considering that part of the particles in direct contact with the carbon support is not accessible to hydrogen adsorption. CV data [66] provide further indication on the difference between the two samples. Maruyama and Abe [70] showed that carbon surface functional groups like quinone contribute in determining the shape of CV curves in acid medium. The CV curve of Pt/CNT_{d} shows clearly this contribution, which is instead minimal in Pt/CNT_{nd}, confirming that ball milling induces the formation of a large number of surface defects on CNT.

The presence of defects, however, does not influence only the size and dispersion of Pt particles [66]. An important aspect regards the efficiency of the three phase boundary, and particularly the efficiency of the transport of protons generated during the H_2 oxidation (see also Fig. 5). The contact between the Pt/CNT and the Nafion membrane is not easy to estimate, but in SEM images of the assembled electrode (MEA – membrane electrode assembly) it is possible to measure the ratio between EDX intensities of Pt and F (Nafion is a sulfonated tetrafluoroethylene based fluoropolymer-copolymer). By averaging the measure over several local spots, it is possible to have an indication of the effectiveness of the contact. The results in Table 1 show that this ratio is about 40% higher in Pt/CNT_{d} with respect to Pt/CNT_{nd}. This is due to the presence of a higher number of defects and associated functional groups in the former allowing a better contact with the Nafion.

Another important aspect to consider is the electron transfer resistance of the CNT substrate, which influences the charging effect of the Pt nanoparticles during high current density operations (see Fig. 5). Direct measurements are difficult, but an estimation of this aspect derives by analysis of the polarization curves in single-cell experiments using a modified Tafel plot [71]. In this equation, the parameter R (polarization resistance) is related to the ohmic resistance in the electrode and electrolyte responsible for the linear variation of potential vs. current density plot. This parameter may be calculated by fitting the polarization curves with the Tafel equation. The value of R estimated with this procedure is reported in Table 1 and is about 25% higher for the PT/CNT_{nd} with respect to Pt/CNT_{d}.

R depends on many parameters: the membrane ionic resistance, the ionic resistance of the electrodes, the electronic resistance of the cell, contact resistance, mass transfer resistance, and the resistance of the carbon substrate. Since all of the MEA components and test fixtures were the same except for the use of ball-milling pretreatment of CNT, it is possible to assume that the difference is due to changes in the electron conduction of the carbon substrate, because induces a polarization in the charge delocalization of Pt supported nanoparticles. This is not a proof of this aspect, but is indicative that also this parameter probably contributes in determining the overall behaviour.

Therefore, the nature of CNT and the presence of defects influence many aspects, not only the dispersion of Pt and the related electrochemically active surface. There is an influence on the (i) efficiency of the contact with Nafion and thus on the proton transfer and effectiveness of the three phase boundary (indicated by the difference in Pt/F ratio), (ii) resistance to electron transfer (suggested by the different value of the parameter R), and (iii) specific characteristics of Pt particles. The latter parameter depends on the size and habit of the metal particles, e.g. on the dispersion and the carbon substrate-metal particle interaction. In

Table 1
Electrochemical active surface area (EAS) determined from cyclic voltammetry experiments, geometrical surface area (GSA) estimated on the basis of the mean diameter of Pt particles or of the size distribution determined by TEM measurements, and mean value of the ratio of the EDX peak intensities of F and Pt in SEM images of Pt/CNT/CC/Nafion composite. Adapted from Ref. [66].

Sample	EAS (m^2/g)	GSA (m^2/g)		F/Pt[a]	R (V/mA)[b]
		Based on mean diameter	Based on size distribution		
Pt/CNT_{d}	163.3	200.3	207.6	1.3	3.33e−3
Pt/CNT_{nd}	114.3	93.5	151.8	0.8	4.49e−3

[a] Average value of about 20 measurements (different spot zones) of the local ratio between the intensities of the EDX peaks of F (related to Nafion) and of Pt in SEM measurements of MEA.
[b] R value (ohmic resistance) in Tafel plot.

fact, the MPD determined in single-cell experiments with pure H_2 and O_2 feeds at anode and cathode sides show a value about 65% higher for Pt/CNT_d with respect to Pt/CNT_{nd} [66]. The increase in the maximum power density is significantly larger than that expected from the differences in the electrochemical surface area (Table 1), confirming that additional effects are present.

Many aspects thus contribute on the single-cell behaviour, evidencing the complexity of the phenomena to consider in analyzing the use of carbon nanotubes for preparation of advanced electrodes. The results also evidence that specific attention should be paid to the role of defects, taking into account their influence on many aspects of the physical electrochemistry of these materials, and not only on the dispersion of Pt particles, as often assumed.

4. Converting CO_2 to fuels using nanoconfined carbon electrodes

Carbon dioxide is a resource and a business opportunity rather than a waste with a cost of disposal [72]. Increasing amounts of low-cost, relatively pure CO_2 will be available in the near future from the many current and planned plants and projects for carbon dioxide sequestration and storage (CSS). Therefore, carbon dioxide can be a feedstock of nearly zero (or even negative) cost for conversion to fuels and chemicals. Valorisation of CO_2 emissions could be one important part of a multifaced strategy for reduction of CO_2 emissions in the atmosphere. Although margins to increase the share of CO_2 recycle for the production of chemicals still exists [73], the volume of CO_2, which can be converted to chemicals, will remain marginal with respect to the emissions. Therefore, a larger contribution to the reduction of CO_2 emissions could derive only by converting CO_2 back to fuels [74,75].

There are several possibilities to convert carbon dioxide to fuels [72]:

(i) by reaction with H_2, for example (a) Reverse Water Gas Shift coupled with methanol synthesis, (b) hydrogenation to light alkanes or alkenes, or (c) hydrogenation to other oxygenates (dimethyl ether, ethanol, formic acid);
(ii) by reaction with hydrocarbons, for example (a) dry, mixed or tri-reforming of methane or (b) use of CO_2 for the alkane oxidative dehydrogenation.

Other possibilities include biological processes (particularly with microalgae), microwave and plasma processes and photo- and electro-chemical/catalytic conversion of CO_2 [72a]. In perspective, the latter is the preferable solution, because uses a renewable source of energy (solar light) to convert carbon dioxide back to fuels. The target is the formation of liquid fuels, because they are and will remain the preferable way to store and transport energy. In addition, the possibility to convert CO_2 to liquid fuels will preserve the current large investments made in energy infrastructures.

Nanoconfined carbon-based electrodes play a relevant role to achieve this objective. We proposed a novel concept for the conversion of CO_2 to fuels based on a gas-phase photoelectrocatalytic (PEC) device [76,77]. PEC reactor is different from the conventional photoelectrochemical approach, based on liquid phase operations. In PEC device, one side (photocatalytic cathode) is composed from a nanostructured TiO_2-based thin film [78], where gaseous water is splitted using solar light to produce O_2, protons and electrons. On the electrocatalytic anode side, based on novel nanostructured carbon based electrodes, CO_2 in the gas phase is converted using the protons and electrons coming from the photocatalytic side and passing through a Nafion membrane and a wire, respectively.

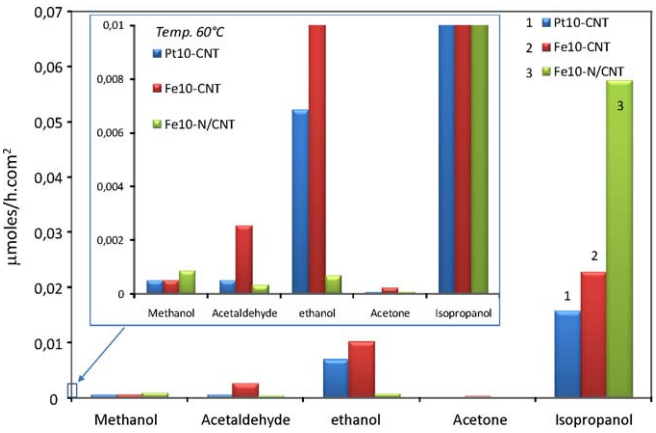

Fig. 6. Comparison of the product distribution in CO_2 electrocatalytic reduction at 60 °C on Pt/CNT, Pt–N–CNT and Fe/CNT (10 wt% in metal).

The key aspect is the electrocatalyst. Recently, various reviews discussed the electrochemical reduction of carbon dioxide [79–81]. Efficiencies in the conversion of electrons higher than 50% require high overpotentials (over 1.5 V). In only few studies, methane or methanol were the primary products of the reduction. The overall yields are low in the absence of high overpotentials and the electrode surface is susceptible to poisoning. All these studies have been made in solution using traditional planar-type electrodes. Using instead a gas-phase approach and nanocarbon based electrocatalysts, we showed that it is possible to form long-chain hydrocarbons at room temperature [82,83], although with low productivities. At higher temperatures (60 °C) better productivities are possible, with the formation in particular of C3 oxygenates (acetone or isopropanol, depending on the electrocatalyst) [84].

Fig. 6 shows the results obtained at 60 °C using three types of electrocatalysts based on Pt or Fe and with a metal loading of 10 wt%. In the case of iron electrocatalysts, the use of CNT or N-doped CNT is also compared. A series of considerations are possible. The first is that isopropanol is the main product of reaction in all cases, although with different productivities. The best is obtained using N-doped CNT, which allows forming about two times more isopropanol, but lower amounts of ethanol and acetaldehyde. Some higher hydrocarbons (up to C8–C9) are also observed, in an amount lower of about two orders of magnitude. The same types of products are observed in the three cases. However, for higher reaction times, the Pt catalyst is more selective toward C1–C2 oxygenated products (in particular, methanol) than the Fe catalyst [84]. The Pt catalyst is also more stable. Note that the electrocatalytic conversion is made at low temperature (60 °C) and 1 bar, while usual higher temperatures (above 200 °C) and pressures (30 bars or more) are necessary for the catalytic conversion of carbon monoxide to higher alcohols and hydrocarbons.

An important aspect is the use of nanocavities, which could favour the consecutive conversion of intermediates with formation of C–C bonds. We should remark that this is a main difference with respect to the "planar-type" conventional electrodes used in the "classical" electrochemical reduction, in addition to the change from liquid to gas phase operations. Carbon black is also active in the reaction, due to the presence of nanopores, but the main product is acetone instead of isopropanol. This is due to the higher acidity of the support. Therefore, the use of CNT instead of carbon black is preferable in terms of type of products (isopropanol is better as fuel component than acetone), but both allow to obtain products with a longer carbon chain, although productivities are better using the CNT-based materials.

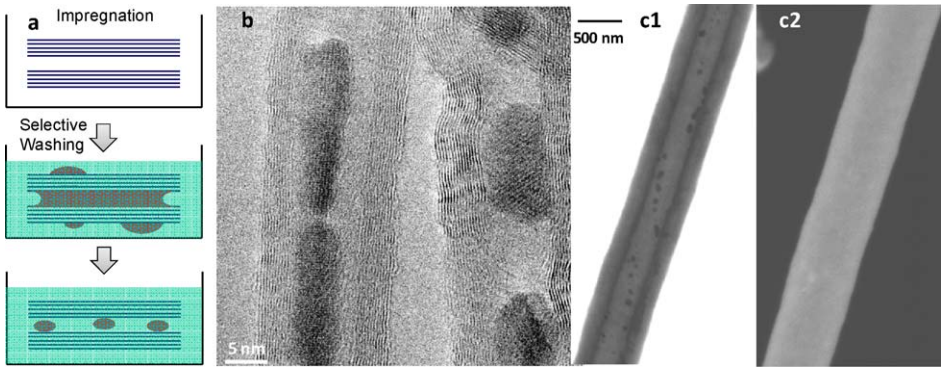

Fig. 7. (a) Cartoon of the procedure of selective filling inside the nanotube (sample Fe@CNT#2).
(b) TEM image of Fe@CNT#2 evidencing that elongated iron particles are present inside the CNT. (c) SEM images of Fe@CNT#2: (c1) transmission mode with 30 keV, i.e. bulk measurements; (c2) secondary electron mode with 1.5 keV, i.e. surface sensitive analysis.

Electron micrographs of both Pt/CNT and Fe/CNT materials show the presence of metal particles both on the inner and outer surface of the nanotubes. The question is whether the localization of the metal particles inside could be useful to promote the conversion of CO_2 to longer carbon chain products. At the FHI-MPG Institute in Berlin (Germany) a method was developed to selectively deposit iron inside carbon nanotubes [85]. The method, based on capillarity and surface tension, is schematically shown in Fig. 7. It consists of two-steps of impregnation and selective washing. By choosing the impregnation and washing solution properly, metal particles are deposited exclusively inside the nanotubes. Specifically, Fe@CNT (iron only inside the carbon nanotube) is produced by impregnation of CNT with a $Fe(NO_3)_3$ aqueous solution and then washing with an immiscible organic solution. TEM images (Fig. 7b) evidence that only elongated iron particles are present inside the CNT. SEM images (Fig. 7c1: transmission mode with 30 keV, i.e. bulk measurements; Fig. 7c2: secondary electron mode with 1.5 keV, i.e. surface sensitive analysis) confirm that the location of these metal particles is only inside the carbon nanotubes.

Fig. 8 reports the comparison of the behaviour at 25 °C in the electrocatalytic reduction of CO_2 of two 10 wt% Fe/CNT samples. In the first catalyst, the iron particles are located on both the inner and outer surface of the CNT (the usual situation). In the second sample, Fe is localized only inside the CNT. The inside localization leads to an enhanced productivity and influences the product distribution. Larger iron particles are present inside the CNT. Fig. 7

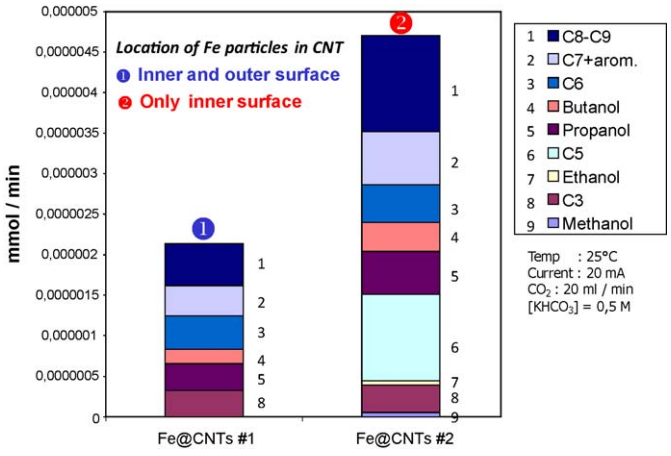

Fig. 8. Comparison of the product distribution in CO_2 electrocatalytic reduction at 25 °C on Fe@CNT (10 wt%. Fe): the iron particles are located both on the inner and outer surface of CNT (#1) or only on the inner surface (#2).

shows the presence of round-shaped particles with size ranging from 2 to 6 nm together with some elongated particles. Outside the CNT, the iron particles range from 1 to 3 nm. Tomography (3D-TEM) confirmed that the biggest nanoparticles were located only inside the nanotube, whereas the smallest decorate the outer surface [84].

We observed [84] that for iron the most active samples showed a core-shell structure in the nanoparticles, with the core reduced (metallic Fe) and an outer shell with composition close to Fe_3O_4. This structure is possible only for particles above a critical size. On the other hand, it has been reported recently that the reduction of Fe_2O_3 nanoparticles is significantly facilitated inside CNTs compared to those on the outside [86]. In situ HRTEM indicated that the CNT-confined Fe_2O_3 particles transformed to metallic iron at 600 °C, while the outside particles remained oxidic at this temperature. The same authors [87] reviewed recently the concept of redox properties modification of transition metals via confinement within the channels of carbon nanotubes and the consequent possibility of tuning their catalytic performance. They also showed [88] that confinement within carbon nanotubes modifies the reactivity of iron catalysts in Fischer-Tropsch synthesis (FTS). The iron species encapsulated inside CNT prefer to exist in a more reduced state, tending to form more iron carbides under the reaction conditions. The latter have been recognized to be essential to obtain high FTS activity. The relative ratio of the integral XRD peaks of iron carbide (Fe_xC_y) to oxide (FeO) is about 4.7 for the encapsulated iron catalyst in comparison to 2.4 for the iron catalyst dispersed on the outer walls of CNTs. This causes a remarkable modification of the catalytic performance. The yield of C5+ hydrocarbons over the encapsulated iron catalyst is twice that over iron catalysts outside CNT and more than six times that over activated-carbon-supported iron catalysts.

In the syngas conversion to C2 oxygenates such as ethanol, acetic acid and acetaldehyde, Rh–Mn particles located inside the CNT show a higher activity than when located on the outer surface [89]. RhMn in the CNT interior likely exists in a more reduced state than that on the exterior and this fact modifies the mechanism of CO adsorption, as evidenced by Raman spectroscopy [89].

Therefore, these studies show that the CNT channels provide a confined reaction environment for catalytic reactions, which is different from that present in microporous materials (zeolites), where spatial restriction on the metal particles and shape-selectivity effects are present. The size is similar to that of mesoporous silica materials (SBA-15) and as demonstrated for them [90–92] reactant confinement effects (pseudo-enhancement of local pressure) could be present. However, inside CNT, the redox properties of metal catalysts are also modified due to the interaction of the metal particles with the interior CNT surfaces.

Due to sp^2 character of carbon atoms and curvature effects, this interaction is very different from that present in silica-based materials. It was demonstrated theoretically that the nature of Pt nanoclusters supported on graphitic carbon, i.e. the Pt–Pt distance, is affected from the interaction with the substrate. In particular, DFT calculations [93] showed that truncated cuboctahedral Pt_{37} clusters supported on graphite evidence the presence of bond length disorder arising from anisotropic distortions in the cluster. The latter is caused by the interactions of the bottom metal particle with the graphite surface.

For this reason, the properties of metal nanoparticles inside the CNT channels could show a different redox behavior. Pan and Bao [87] clearly demonstrated that the reduction of metal oxides is facilitated inside CNT with respect to those on the CNT exterior surfaces and the extent of facilitation depends on the CNT diameters. In addition, the oxidation of CNT-confined metallic iron is retarded.

These properties are important in general, and not only for the specific case of carbon dioxide or carbon monoxide conversion. This provides a novel approach to tune the catalytic behaviour of metal catalysts for reactions, which are sensitive to the electronic state of the active components. Examples cited by Pan and Bao [87] were syngas conversion, hydrogenation/dehydrogenation of hydrocarbons, ammonia synthesis and catalysis in fuel cell. Probably the range of interested reactions is larger, although still to be explored. Note how this concept put a clear link between catalysis and electrocatalysis.

Actual studies of the reaction over CNT nanoconfined catalysts are mainly limited to MWNT, being easier their preparation and lower the cost in comparison to SWNT and DWNT (double walled nanotubes). In addition, having MWNT a larger internal diameter, the introduction of metal nanoparticles is relatively easier. As noted by Pan and Bao [87], SWNT and DWNT are more interesting for this application from the structural property point of view, because they have a higher degree of uniformity since they consist of only one or two graphene sheets with fewer defects. In addition, their diameter distribution is generally narrower (range of 1–3 nm). Furthermore, the carbon sp^2 hybridization becomes more deformed in SWNT and DWNT, because of their large curvatures [94], which could lead to a stronger interaction with metals.

5. Conclusions

The use of nanostructured carbon-based electrodes for clean and sustainable energy production is a topic of increasing relevance both from the application and fundamental points of view. There are increasing publications on this area, which is relevant for the development of both advanced catalysts and electroactive materials. This short review did not analyze analytically the progresses in this field, but instead attempted to critically highlight some selected issues or aspects. As summarized below, three aspects have been commented.

The nanodesign of electrodes is of growing relevance for the optimization of the reaction and mass transport kinetics, but the opportunities go beyond to only these aspects. The control and optimization of the nanostructure, especially in carbon-metal oxide hybrid materials, is a critical issue, but many aspects have to be considered. We have commented some of these aspects by comparing the synthesis method by the hard template approach with respect to that based on a CNT array produced by the CVD method. A further possibility is given by structuring the inner nanospace of carbon nanotubes, e.g. nano-in-nano design. The preparation of carbon-tube-in-tube or CNF confined within CNT has been discussed as an example, although it was also evidenced that their application to prepare advanced electrodes for Li-ion batteries still require further studies.

The problem of nanointerfaces and charge transport has been discussed in relation to the electrodes for PEM fuel cells. Moreover, the issue of the interrelation between dynamics of surface reconstruction of Pt nanoparticles under operation conditions and charge transport limitations was evidenced. This is an area which needs more in-depth studies. The limits in considering the ORR as the only critical element in PEM electrodes design have been also commented. Finally, the need to take into account multiple complex and interconnected effects in the evaluation of the performances of novel advanced electrodes for PEM fuel cells has been analyzed with a specific example on the influence of mechanically-induced defects on CNT on the performances of Pt/CNT/CC electrodes.

The final part was dedicated to shortly discuss the use of advanced nanostructured carbon-based electrodes for the electrocatalytic reduction of CO_2 to fuels. The concept of transformation of carbon dioxide back to liquid fuels (isopropanol, in particular) is proof, but still significant developments are necessary before to apply this option. This reaction is an example of an area only recently investigated, promising for the field of both catalysis and electrocatalysis. In fact, it evidences that a modification in the redox properties of transition metals via nanoconfinement within the channels of carbon nanotubes is possible, with a consequent possibility of tuning their catalytic performance. New possibilities in controlling the (electro)catalytic behavior are open, although further studies are necessary to put them on a more general bases.

In conclusion, a close relationship between catalysis and electrocatalysis exists, although some relevant differences should be considered in their respective material design. In both cases, there are examples showing how the control of the nano-structure and -architecture can lead to a significant progress, which may be immediately exploited in terms of improved performances for a cleaner and sustainable energy production. Carbon-based materials are a key component of electrodes, for the high electronic conductivity, robustness and rich functional surface chemistry of carbon. The same properties are also relevant for catalysis, but less used in comparison to the electrode case. It is thus time to strengthen the effort in an advanced design of carbon based catalytic materials, taking into account all the advances made in the field of electrodes development.

Acknowledgements

This contribution was realized in the frame of the activities of the Network of Excellence IDECAT (NMP3-CT-2005-011730) and of the ELCAT project (FP6-2003-NEST-A/2400), both supported from the European Commission. The collaboration with Dr. D.S. Su, Dr. J-P. Tessonnier and prof. R. Schlögl (Berlin), Dr. C. Pham-Huu and prof. J.M. Ledoux (Strasbourg), in particular, within the above projects and the common European Laboratory for Surface Science and Catalysis (ELCASS) is gratefully acknowledged.

References

[1] G. Centi, R.A. van, Santen (Eds.), Catalysis for Renewables, Wiley VCH Pub, Weinheim (Germany), 2007.
[2] C. Bianchini, P. Barbaro (Eds.), Catalysis for Sustainable Energy Production, Wiley VCH Pub, Weinheim (Germany), 2009.
[3] R.L. McCreery, Chem. Rev. 108 (2008) 2646.
[4] A.L. Dicks, J. Power Sources 156 (2006) 128.
[5] J. Yan, H. Zhou, P. Yu, L. Su, L. Mao, Adv. Mater. 20 (2008) 2899.
[6] C. Liu, H.-M. Cheng, J. Phys. D: Appl. Phys. 38 (2005) R231.
[7] E. Frackowiak, F. Beguin, Carbon 39 (2001) 937.
[8] J.J. Gooding, Electrochim. Acta 50 (2005) 3049.
[9] D.R. Rolison, J.W. Long, J.C. Lytle, A.E. Fischer, C.P. Rhodes, T.M. McEvoy, M.E. Bourg, A.M. Lubers, Chem. Soc. Rev. 38 (2009) 226.
[10] Y. Xie, C. Wu, Dalton Trans. 45 (2007) 5235.
[11] F. Patolsky, Science 317 (2007) 320.
[12] A.L. Briseno, S.C.B. Mannsfeld, M.M. Ling, S.H. Liu, R.J. Tseng, C. Reese, M.E. Roberts, Y. Yang, F. Wudl, Z.N. Bao, Nature 444 (2006) 913.

[13] Y.-G. Guo, J.-S. Hu, L.-J. Wan, Adv. Mater. 20 (15) (2008) 2878.
[14] J. Liu, G. Cao, Z. Yang, D. Wang, D. Dubois, X. Zhou, G.L. Graff, L.R. Pederson, J.-G. Zhang, ChemSusChem 1 (8–9) (2008) 676.
[15] K. Lee, J. Zhang, H. Wang, D.P. Wilkinson, J. Appl. Electrochem. 36 (5) (2006) 507.
[16] R.W. Murray, Chem. Rev. 108 (2008) 2688.
[17] Y. Yamanoi, H. Nishihara, Chem. Commun. (2007) 3983.
[18] C.-C. Chien, K.-T. Jeng, Mater. Chem. Phys. 103s (2–3) (2007) 400.
[19] S. Sun, F. Jaouen, J.-P. Dodelet, Adv. Mater. 20 (2008) 3900.
[20] M.S. Saha, R. Li, X. Sun, S. Ye, Electrochem. Commun. 11 (2009) 438.
[21] J. Yang, D.-J. Liu, Carbon 45 (2007) 2845.
[22] A. Guha, W. Lu, T.A. Zawodwzinski Jr., D.A. Schiraldi, Carbon 45 (2007) 1506.
[23] Y. Shao, J. Sui, G. Yin, Y. Gao, Appl. Catal. B: Environ. 79 (2008) 89.
[24] D. Vairavapandian, P. Vichchulada, M.D. Lay, Anal. Chimica Acta 626 (2008) 119.
[25] M. Michel, A. Taylor, R. Sekol, P. Podsiadlo, N. Kotov, L. Thompson, Adv. Mater. 19 (2007) 3859.
[26] G. Centi, S. Perathoner, Eur. J. Inorg. Chem. (2009) 3851 (minireview).
[27] G. Centi, G. Cum, J.L.G. Fierro, J.M. López Nieto, Direct Conversion of Methane, Ethane and Carbon Dioxide to Fuels and Chemicals, CAP Report, The Catalyst Group Resources, 2008.
[28] A.T. Bell, B.C. Gates, D. Ray, Basic Research Needs: Catalysis for Energy (PNNL-17214), U.S. Department of Energy, Report from a Workshop held in August 6–8, 2007, in Bethesda, Maryland (US) (www.sc.doe.gov/bes/reports/list.html).
[29] S. Niyogi, M.A. Hamon, H. Hu, B. Zhao, P. Bhowmik, R. Sen, M.E. Itkis, R.C. Haddon, Acc. Chem. Res. 35 (2002) 1105.
[30] T.W. Odom, J.L. Huang, P. Kim, C.M. Lieber, J. Phys. Chem. B 104 (2000) 2794.
[31] (a) J. Lee, J. Kim, T. Hyeon, Adv. Mater. 18 (16) (2006) 2073;
(b) W.B. Choi, B.H. Cheong, J.J. Kim, J. Chu, E. Bae, Adv. Funct. Mater. 13 (2003) 80.
[32] S. Zhao, H. Roberge, A. Yelon, T. Veres, J. Am. Chem. Soc. 128 (2006) 12352.
[33] G. Drobychev, A. Barysevich, K. Delendik, P. Nedelec, D. Sillou, O. Voitik, Nuclear Instr. Meth. A (2009) doi:10.1016/j.nima.2009.05.076.
[34] A.L.M. Reddy, M.M. Shaijumon, S.R. Gowda, P.M. Ajayan, Nano Lett. 9 (3) (2009) 1002.
[35] A.S. Arico, P. Bruce, B. Scrosati, J.M. Tarascon, W. Van Schalkwijk, Nat. Mater. 4 (2005) 366.
[36] J. Maier, Nat. Mater. 4 (2005) 805.
[37] Y. Wang, G.Z. Cao, Adv. Mater. 20 (2008) 2251.
[38] G.L. Che, B.B. Lakshmi, E.R. Fisher, C.R. Martin, Nature 393 (1998) 346.
[39] E. Frackowiak, S. Gautier, H. Gaucher, S. Bonnamy, F. Beguin, Carbon 37 (1999) 61.
[40] G.T. Wu, M.H. Chen, G.M. Zhu, J.K. You, Z.G. Lin, X.B. Zhang, J. Solid State Electrochem. 7 (2003) 129.
[41] J.Y. Eom, H.S. Kwon, J. Liu, O. Zhou, Carbon 42 (2004) 2589.
[42] L. Dai, Adv. Appl. Ceram. 107 (4) (2008) 177.
[43] P. Launois, P. Poulin, Macroscopically aligned carbon nanotubes, in: N.H. Singh (Ed.), Encyclopedia of Nanoscience and Nanotechnology, vol. 4, American Scientific Publishers, Stevenson Ranch, California, 2004, p763.
[44] C.R. Sides, N. Li, C.J. Patrissi, B. Scrosati, C.R. Martin, MRS Bull. 27 (8) (2002) 604.
[45] A. Singhal, G. Skandan, G. Amatucci, F. Badway, N. Ye, A. Manthiram, H. Ye, J.J. Xu, J. Power Sources 129 (1) (2004) 38.
[46] D. Sun, C.W. Kwon, G. Baure, E. Richman, J. MacLean, B. Dunn, S.H. Tolbert, Adv. Functional Mater. 14 (12) (2004) 1197.
[47] J.W. Fergus, J. Mater. Sci. 38 (21) (2003) 4259.
[48] I.-H. Kim, J.-H. Kim, B.-W. Cho, Y.-H. Lee, K.-B. Kim, J. Electrochem. Soc. 153 (6) (2006) A989.
[49] W.-C. Fang, W.-L. Fang, Chem. Commun. (41) (2008) 5236.
[50] X.-W. Chen, Z. Zhu, M. Haevecker, D.S. Su, R. Schlögl, Mater. Res. Bull. 42 (2) (2007) 354.
[51] Y. Tu, Z.P. Huang, D.Z. Wang, J.G. Wen, Z.F. Ren, Appl. Phys. Lett. 80 (21) (2002) 4018.
[52] P. Lanzafame, S. Perathoner, G. Centi, F. Frusteri, J. Porous Mater. 14 (3) (2007) 305.
[53] Z. Zhu, D.S. Su, G. Weinberg, R.E. Jentoft, R. Schlögl, Small 1 (1) (2005) 107.
[54] J. Zhang, Y.-S. Hu, J.-P. Tessonnier, G. Weinberg, J. Maier, R. Schlögl, D.S. Su, Adv. Mater. 20 (2008) 1450.
[55] Y.-S. Hu, X. Liu, J.-O. Müller, R. Schögl, J. Maier, D.S. Su, Angew. Chemie, Int. Ed. 48 (1) (2009) 210.
[56] R. de Miguel, J. Phys. Chem. B 110 (2006) 8176.
[57] L. Zhu, R. Wang, T.S. King, A.E. DePristo, J. Catal. 167 (1997) 408.
[58] A.A. Franco, S. Passot, P. Fugier, C. Anglade, E. Billy, L. Guetaz, N. Guillet, S. Mailley, ECS Trans. 13 (17) (2008) 29.
[59] G.H. Hoogers, in: G. Hoogers (Ed.), Fuel Cell Technology Handbook, CRC Press, Boca Raton (US), 2003, , Ch. 4, p. 88.
[60] A. Witkowska, E. Principi, A. Di Cicco, S. Dsoke, R. Marassi, L. Olivi, M. Centazzo, A.R. Albertini, J. Non-Crystalline Solids 354 (35–39) (2008) 4227.
[61] M. Tada, S. Murata, T. Asakoka, K. Hiroshima, K. Okumura, H. Tanida, T. Uruga, H. Nakanishi, S.-i. Matsumoto, Y. Inada, M. Nomura, Y. Iwasawa, Angew. Chemie, Int. Ed. 46 (23) (2007) 4310.
[62] H. Kageyama, T. Ioroi, T. Kojima, H. Senoh, N. Takeichi, K. Nomura, K. Tanimoto, AIP Conference Proceedings 882 (X-Ray Absorption Fine Structure (XAFS13)), 2007, p. 645.
[63] S.B. Adler, Chem. Rev. 104 (2004) 4791.
[64] Y. Shao, J. Liu, Y. Wang, Y. Lin, J. Mater. Chem. 19 (2009) 46.
[65] G. Centi, S. Perathoner, Topics Catal. 52 (8) (2009) 948.
[66] G. Centi, M. Gangeri, M. Fiorello, S. Perathoner, J. Amadou, D. Bégin, M.J. Ledoux, C. Pham-Huu, M.E. Schuster, D.S. Su, J.-P. Tessonnier, R. Schlögl, Catal. Today 147 (2009) 287.
[67] J.-H. Ahn, H.-S. Shin, Y.-J. Kim, H. Chung, J. Alloys Compd. 434–435 (2007) 428.
[68] K.-D. Cai, G.-P. Yin, J.-J. Wang, K.-L. Lu, Energy Fuels 23 (2009) 903.
[69] A. Pozio, M.D. Francesco, A. Cemmi, F. Cardellini, I. Giorgi, J. Power Source 105 (2002) 13.
[70] J. Maruyama, I. Abe, Electrochim. Acta 46 (2001) 3381.
[71] M.S. Saha, R. Li, X. Sun, J. Power Source 7 (2008) 314.
[72] (a) G. Centi, G. Cum, in Direct Conversion of Methane, Ethane and Carbon Dioxide to Fuels and Chemicals, CAP Report, J.L.G. Fierro, J.M. López Nieto (Eds.), The Catalyst Group Resources, 2008.
(b) G. Centi, S. Perathoner, Catal. Today 148 (2009) 191.
[73] M. Aresta, A. Dibenedetto, Dalton Trans. 28 (2007) 2975.
[74] G. Centi, S. Perathoner, Stud. Surf. Sci. Catal. 153 (2004) 1 (Carbon Dioxide Utilization for Global Sustainability).
[75] E.E. Benson, C.P. Kubiak, A.J. Sathrum, J.M. Smieja, Chem. Soc. Rev. 38 (2009) 89.
[76] G. Centi, S. Perathoner, Z. Rak, Stud. Surf. Sci. Catal. 145 (2003) 283.
[77] G. Centi, S. Perathoner, Z. Rak, Appl. Catal. B: Env. 41 (2003) 143.
[78] S. Perathoner, R. Passalacqua, G. Centi, D.S. Su, G. Weinberg, R. Schlögl, Catal. Today 122 (2007) 3.
[79] J.-L. DuBois, DuBois, Electrochemical reactions of carbon dioxide, Encyclopedia Electroche. vol. 7 (2006) 202.
[80] M. Gattrell, N. Gupta, A. Co, J. Electroanal. Chem. 594 (2006) 1.
[81] C. Oloman, H. Li, ChemSusChem 1 (2008) 385.
[82] G. Centi, S. Perathoner, G. Winè, M. Gangeri, Converting CO_2 to fuel: a dream or a challenge? Preprints of Symposia – American Chemical Society, Div. Fuel Chem. 51 (2006) 745.
[83] G. Centi, S. Perathoner, G. Wine, M. Gangeri, Green Chem. 9 (2007) 671.
[84] M. Gangeri, S. Perathoner, S. Caudo, G. Centi, J. Amadou, D. Bégin, C. Pham-Huu, M.J. Ledoux, J.-P. Tessonnier, D.S. Su, R. Schlögl, Catal. Today 143 (1–2) (2009) 57.
[85] Q. Fu, G. Weinberg, D.S. Su, Xinxing Tan Cailiao 23 (1) (2008) 17.
[86] W. Chen, X. Pan, M.G. Willinger, D.S. Su, X. Bao, J. Am. Chem. Soc. 128 (2006) 3136.
[87] X. Pan, X. Bao, Chem. Commun. (2008) 6271.
[88] W. Chen, Z. Fan, X. Pan, X. Bao, J. Am. Chem. Soc. 130 (29) (2008) 9414.
[89] X. Pan, Z. Fan, W. Chen, Y. Ding, H. Luo, X. Bao, Nat. Mater. 6 (2008) 507.
[90] S. Abate, K. Barbera, P. Lanzafame, S. Perathoner, G. Centi, Preprints – Am. Chem. Soc., Div. Pet. Chem. 53 (1) (2008) 227.
[91] F. Goettmann, C. Sanchez, J. Mater. Chem. 17 (1) (2007) 24.
[92] S. Pariente, P. Trens, F. Fajula, F. Di Renzo, N. Tanchoux, Appl. Catal., A: General 307 (1) (2006) 51.
[93] L.-L. Wang, S.V. Khare, V. Chirita, D.D. Johnson, A.A. Rockett, A.I. Frenkel, N.H. Mack, R.G. Nuzzo, J. Am. Chem. Soc. 128 (2006) 131.
[94] B. Shan, K. Cho, Phys. Rev. B 73 (2006) 081401.